

Supporting Information

Plastic-derived sandwich-like porous carbon nanosheets-supported hexagonal carbon micro-flakes for K-ion storage

Tianci Kong,^a Yong Qian,^b Yang Li,^a Ning Lin^{a,*} and Yitai Qian^{a,b,*}

^aSchool of Chemistry and Materials Science, University of Science and Technology of China, Hefei 230026, P. R. China

^bHefei National Laboratory for Physical Sciences at the Microscale, University of Science and Technology of China, Hefei 230026, P. R. China

E-mail address: ningl@mail.ustc.edu.cn (N. Lin); y tqian@ustc.edu.cn (Y. Qian)

Experimental Section

Materials preparation

Preparation of WPWMC: Firstly, waste polyethylene straws was cut into small piece about 0.5 * 0.5 cm². Then plastic debris (1.5 g), magnesium powder (0.5 g) and ultrapure water (10 mL) were added into a 20 ml stainless steel autoclave. The autoclave was sealed and transferred to the electric furnace with a heating rate of 5 °C min⁻¹ and maintained at 700 °C for 5 h, and then cooled to room temperature naturally. The sample was washed with ultrapure water, ethanol, and hydrochloric acid solution (6 mol L⁻¹) at 100 °C for 12 h, and then dried in vacuum at 80 °C for 5 h.

Preparation of WPC, WPWC, WPMC: The WPC is obtained by directly heating plastic debris (1.5 g) in the autoclave. WPWC is synthesized with plastic debris (1.5 g) and ultrapure water (10 mL) in the stainless-steel autoclave. The WPMC is obtained by heating plastic debris (1.5 g) and magnesium powder (0.5 g) in the autoclave. The other parameters remain unchanged.

Characterization

The structures of the samples were measured by X-ray diffraction (XRD) on a Philips X' Pert Super diffractometer with Cu K α ($\lambda=1.54182$ Å), and Raman spectroscopy was performed by a JYLABRAM-HR Confocal Laser Micro-Raman spectrometer at 532 nm. The morphologies of the samples were characterized on scanning electron microscopy (SEM, JEOL-JSM-6700F), transmission electron microscopy (TEM, Hitachi H7650) and high resolution transmission electron microscopy (HRTEM, JEM-2100F). The surface areas and pore size distribution of the samples were obtained by BEL SORP-max machine (BEL, Japan). Thermogravimetric analysis (TGA) was carried out on Shimadzu TGA-50H. X-ray photoelectron spectroscopy (XPS) was collected on an ESCALAB 250 X-ray photoelectron spectrometer (Perkin-Elmer).

Electrochemical characterization

The electrochemical performances of the samples were measured using CR2016 coin cells with about 150 μ L electrolyte (1.0 M KFSI in ethylene carbonate (EC) and diethyl carbonate (DEC) (1:1, v/v). The electrode was composed of 70 wt.% active materials, 20 wt.% super P, 10 wt.% carboxymethyl cellulose (CMC). The mixed slurry was coated on a copper film and dried at 100 °C for 6 h in a vacuum oven. The mass loading of electrodes was calculated at about 1 mg cm⁻². And the coin cells were assembled in the argon-filled glove box (O₂, H₂O < 0.1 ppm). The discharge and charge measurements were carried out at various current rates in the voltage range of 0.01-2.5 V on a LANDCT2001A battery tester. And the CMK-3 (ordered mesoporous carbon prepared with SBA-15 as the hard template, purchased from Nanjing XFNANO Materials Tech Co., Ltd) electrodes were cycled at 1.2-4.2 V, while PIHCs were cycled at 0.01-4.0 V. Before assembling PIHCs, the WPWMC anodes and CMK-3 cathodes are electrochemically pre-potassiated by cycling 10 cycles at a current density of 1000 mA g⁻¹. The cyclic voltammogram (CV) measurements were performed on a CHI 660D Electrochemical Workstation (Shanghai Chenhua Corp.).

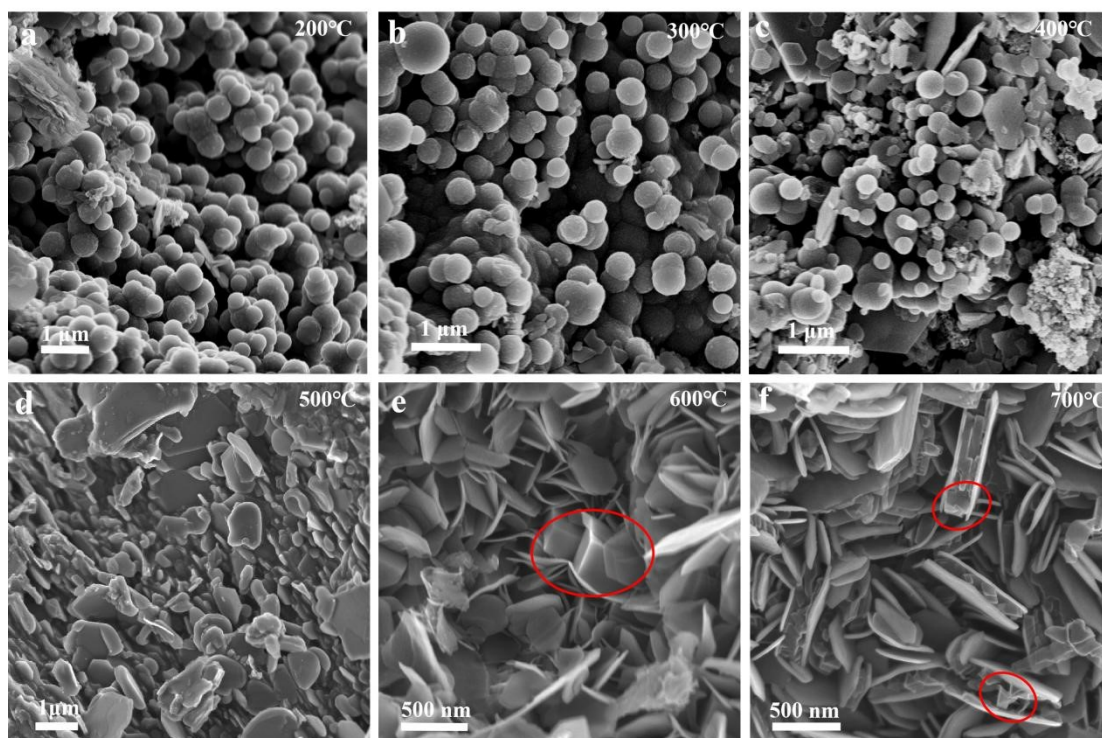


Fig. S1. SEM images of the WPWMC-Ts before HCl treatment.

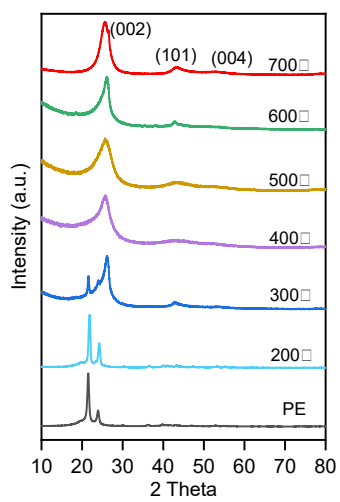


Fig. S2. XRD patterns of PE and the WPWMC-Ts after HCl treatment.

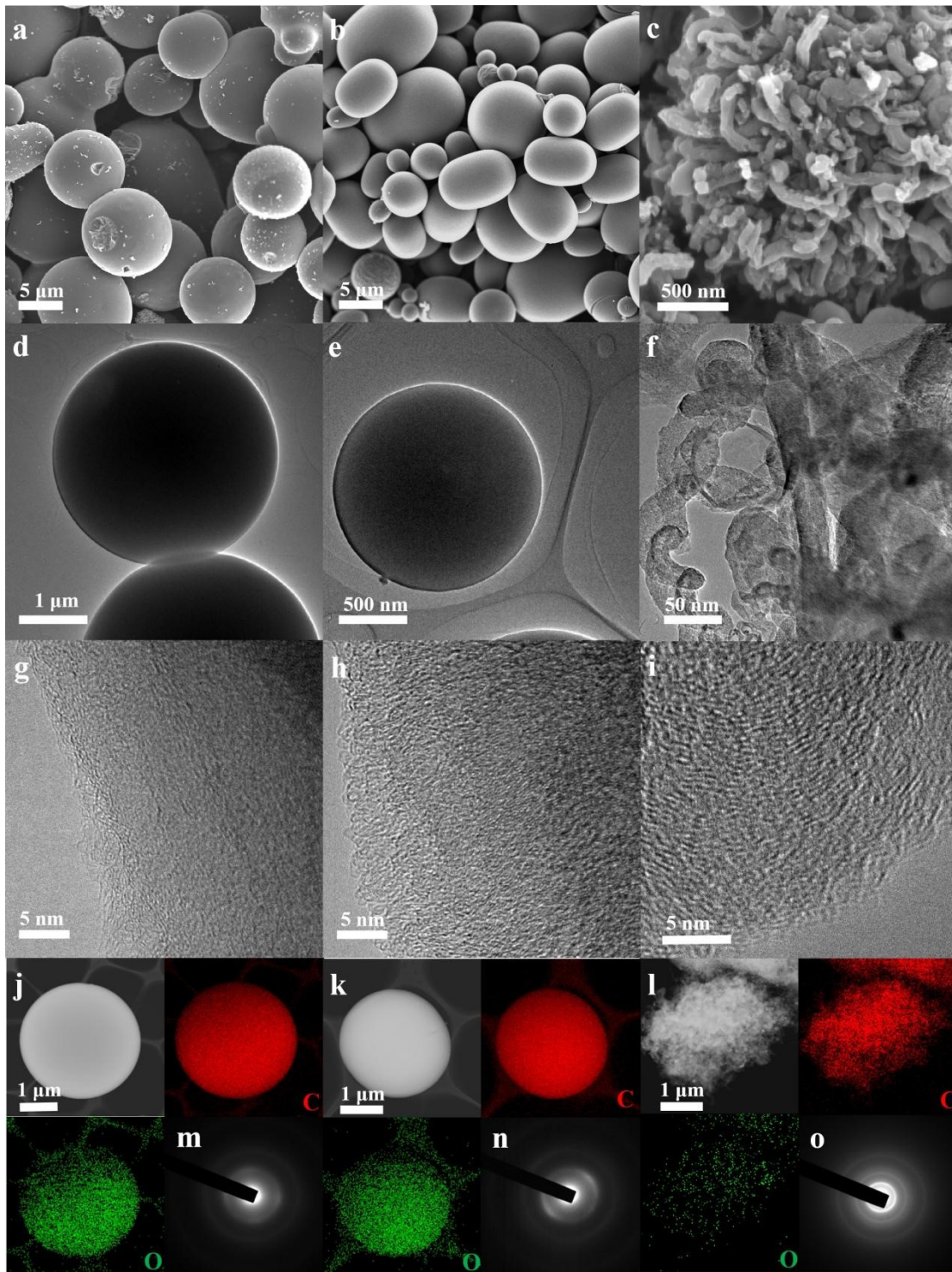


Fig. S3. (a-c) The SEM images of the WPC, WPWC, WPMC. (d-f) The TEM image of the WPC, WPWC, WPMC. (g-i) The HRTEM images of the WPC, WPWC, WPMC. (j-l) The elemental mapping (C, O) images of the WPC, WPWC, WPMC. (m-o) SAED images of the WPC, WPWC, WPMC.

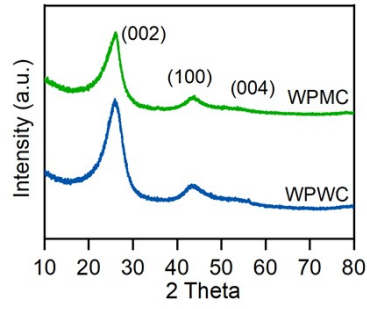


Fig. S4. XRD patterns of the WPWC and WPMC.

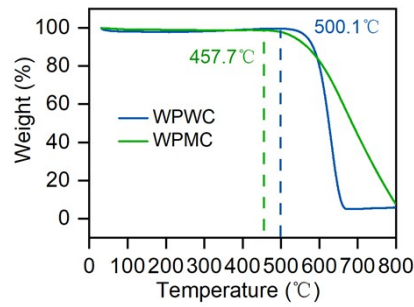


Fig. S5. TGA curves of the WPWC and WPMC in O_2 at a heating rate of $10\text{ }^\circ\text{C min}^{-1}$.

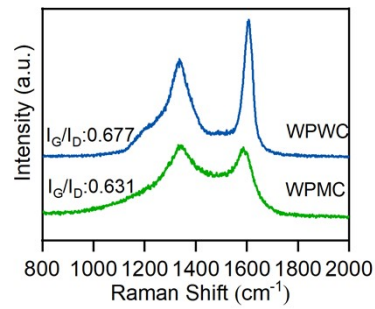


Fig. S6. Raman spectra curves of the WPWC and WPMC.

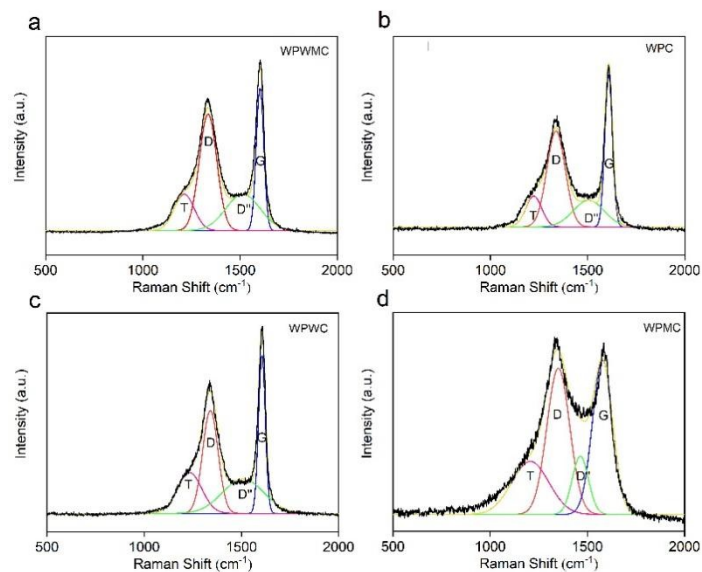


Fig. S7. Fitted Raman spectra curves of (a) WPWMC, (b) WPC, (c) WPWC, (d) WPMC. The red line with a peak at 1335 cm⁻¹ represents the D-band, while the blue line with a peak close to 1600 cm⁻¹ represents the G-band. Integrated ratios are obtained from the area of the fitted peaks. The fitting is made by using the OMNIC Picta software program with a gaussian-laurentzian fit.¹

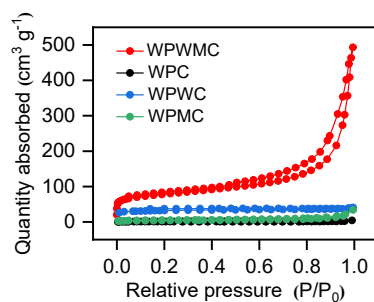


Fig. S8. Nitrogen adsorption-desorption isotherms of the WPWMC, WPC, WPWC and WPMC.

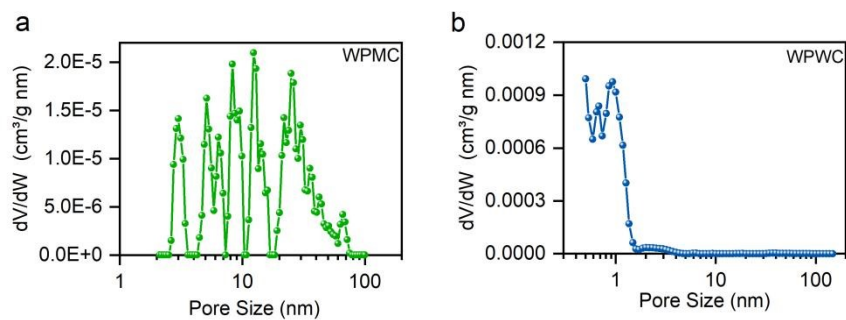


Fig. S9. The pore sizes of (a) WPMC, (b) WPWC.

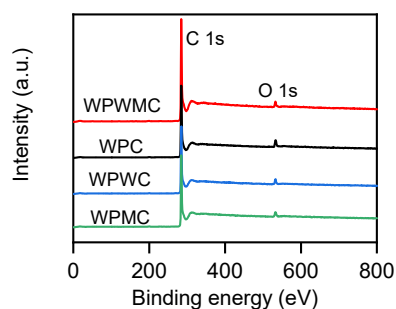


Fig. S10. XPS survey of the WPWMC, WPC, WPWC and WPMC.

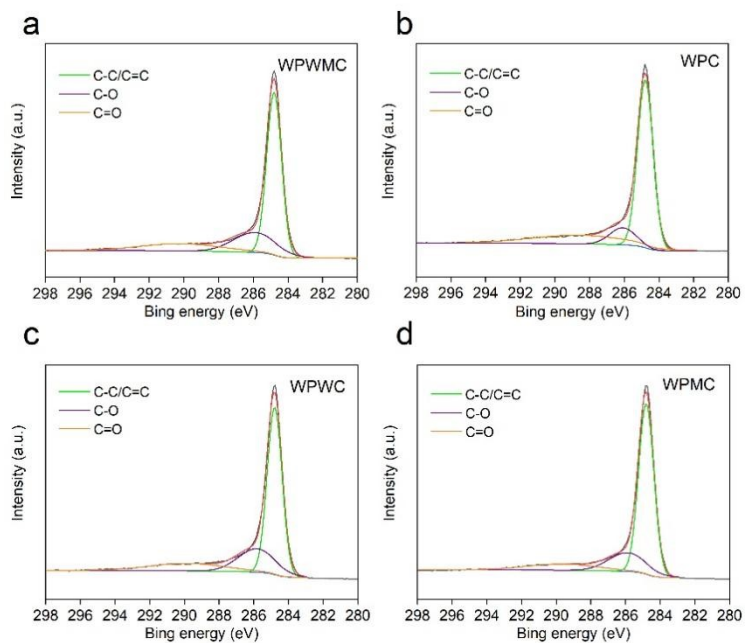


Fig. S11. XPS high-resolution C 1s spectra of the WPWMC, WPC, WPWC and WPMC.²

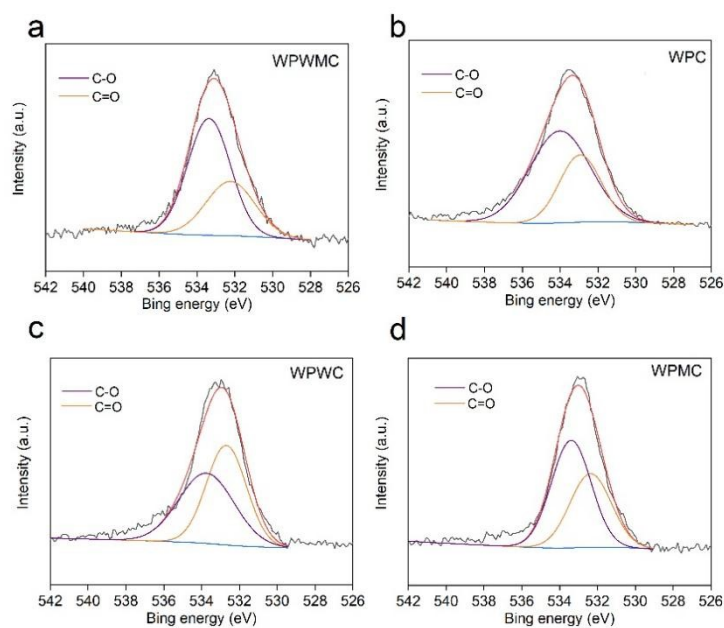


Fig. S12. XPS high-resolution O 1s spectra of the WPWMC, WPC, WPWC and WPMC.³

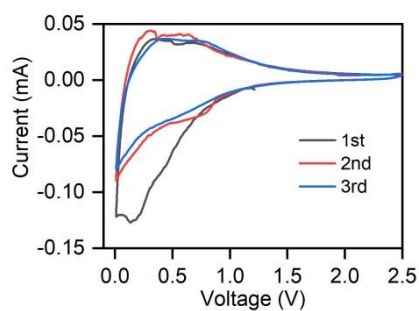


Fig. S13. First three consecutive CV curves of the WPWMC electrode in the voltage range of 0.01-2.5 V at scan rate of 0.1 mV s^{-1} .

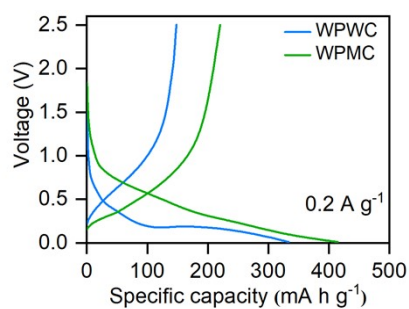


Fig. S14. The first charge-discharge curves of the WPWC and WPMC at 200 mA g^{-1} .

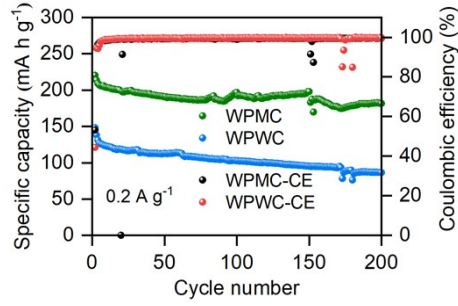


Fig. S15. The cycling performance of the WPWC and WPMC at 200 mA g⁻¹.

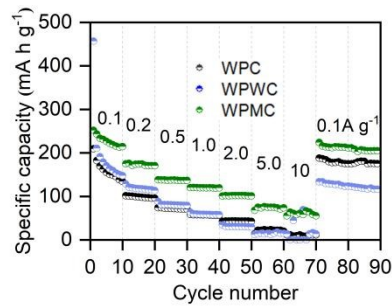


Fig. S16. The rate capabilities at various current rates of the WPC, WPWC and WPMC.

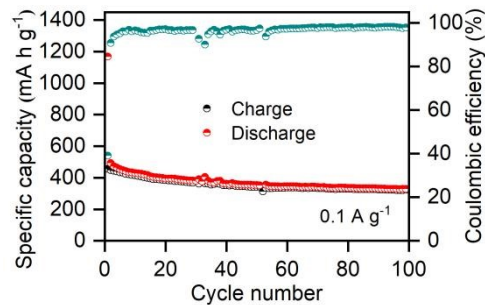


Fig. S17. The cycling performance of the WPWMC at 0.1 A g⁻¹. At the current density of 0.1 A g⁻¹, the WPWMC anode displays a reversible capacity of 329.0 mA h g⁻¹ after 100 cycles.

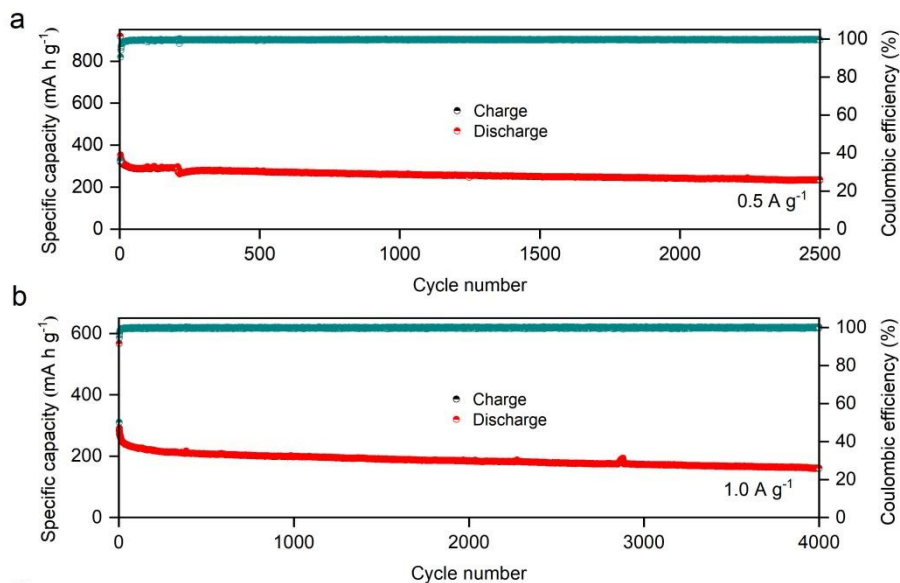


Fig. S18. The cycling performance of the WPWMC at (a) 0.5 A g⁻¹. (b) 1.0 A g⁻¹. The WPWMC anode delivers a capacity of 173.7 mA h g⁻¹ after 2500 cycles at 0.5 A g⁻¹, as well as a capacity of 161.2 mA h g⁻¹ after 4000 cycles at 1.0 A g⁻¹.

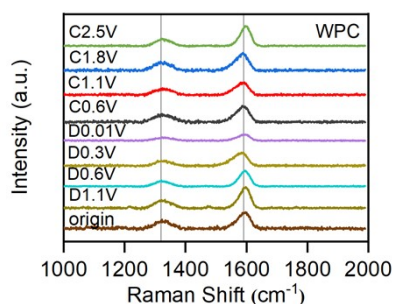


Fig. S19. Ex situ Raman spectra at different discharge/charge states of the WPC.

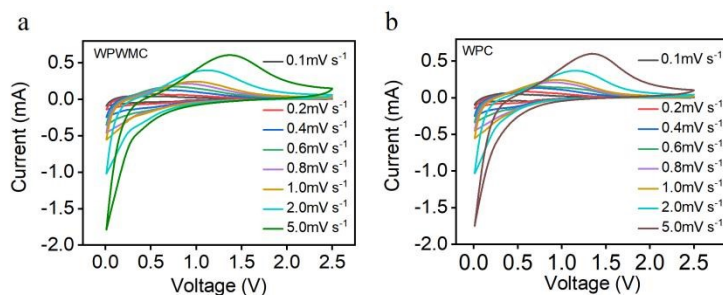


Fig. S20. The CV curves from 0.1 to 5.0 mV s⁻¹ for the WPWMC and WPC.

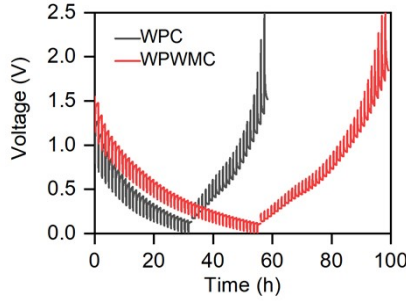


Fig. S21. The GITT curves at the fifth cycle of the WPC and WPWMC at 50 mA g⁻¹.

Ion diffusivity is a key factor of electrode materials for batteries, which links directly to their rate capability. In order to study the influence of the temperature on the ion diffusion coefficients, the GITT method is carried out to measure the samples. Based on the GITT measurement, the potassium ion diffusion coefficients can be calculated by the following equation:⁴

$$D_{K^+} = \frac{4}{\pi} \left(\frac{m_B V_M}{M_B S} \right)^2 \left(\frac{\Delta E_s}{\tau (dE_\tau / d\sqrt{\tau})} \right)^2 \dots (\tau \ll L^2 / D_{K^+})$$

Where V_M (cm³ mol⁻¹) is the molar volume of samples, M_B (g mol⁻¹) and m_B (g) are the molecular weight and mass of the electrode materials, respectively. S (cm²) is the active surface area of the electrode, which is measured by the BET method. L (cm) is the diffusion distance, which is approximately the thickness of the electrode. The equation could be further simplified as:⁵

$$D_{K^+} = \frac{4}{\pi \tau} \left(\frac{m_B V_M}{M_B S} \right)^2 \left(\frac{\Delta E_s}{\Delta E_\tau} \right)^2$$

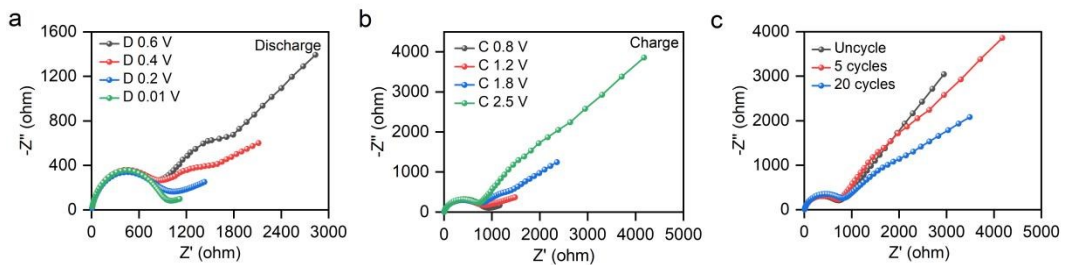


Fig. S22. Nyquist plots of WPWMC at (a) discharge state, (b) charge state, and (c) different cycle numbers.

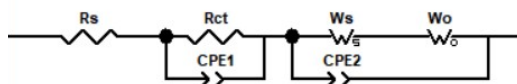


Fig. S23. The equivalent circuit used to fit the experimental data (R_s : solution resistance; R_{ct} : charge-transfer resistance; W_s : adsorption impedance; W_o : semi-infinite Warburg diffusion impedance; CPE1 and CPE2: constant phase element).

Table S1. The simulated data from EIS spectra using the equivalent circuit shown in Fig. S23.

Samples	R_{ct} (Ω)	W_s (Ω)	W_o (Ω)
D 0.6 V	710	2722	907
D 0.4 V	683.1	1826	1226
D 0.2 V	630.8	-	1765
D 0.01 V	614.3	-	1857
C 0.8 V	597.7	-	1630
C 1.2 V	592.5	-	1617
C 1.8 V	579.8	2462	1200
C 2.5 V	573.4	3898	776
Uncycled	711.5	2561	788
5 th cycle	726.6	2628	809
20 th cycle	731.2	2886	861

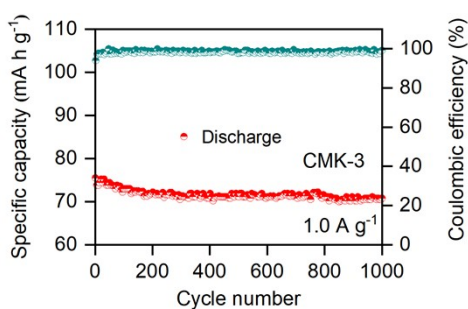


Fig. S24. The cycling performance of the CMK-3 at 1000 mA g^{-1} in the voltage range of 1.2-4.2 V.

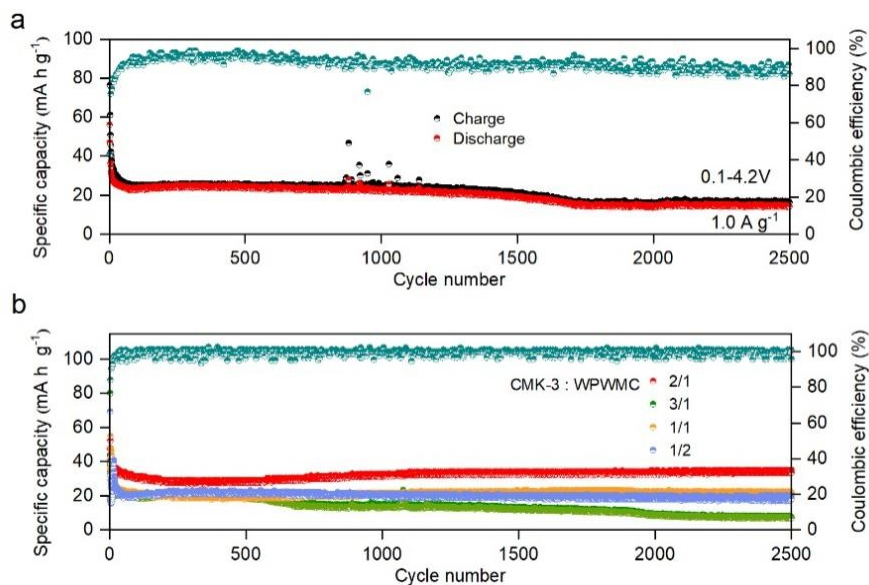


Fig. S25. (a) The cycling performance of the WPWMC//CMK-3 PIHC at 1000 mA g⁻¹ in the voltage range of 0.1-4.2 V. (b) The cycling performance of the WPWMC//CMK-3 PIHC at 1000 mA g⁻¹ with the mass loading ratio CMK-3 and WPWMC at 1/2, 1/1, 2/1, 3/1.

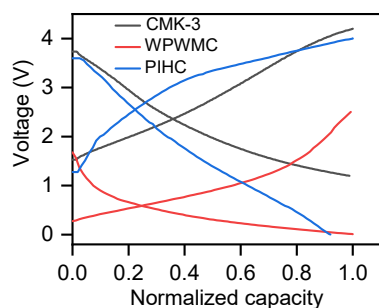


Fig. S26. The 10th charge-discharge curves of the CMK-3 cathode, WPWMC anode, and WPWMC//CMK-3 hybrid capacitor at 1000 mA g⁻¹.

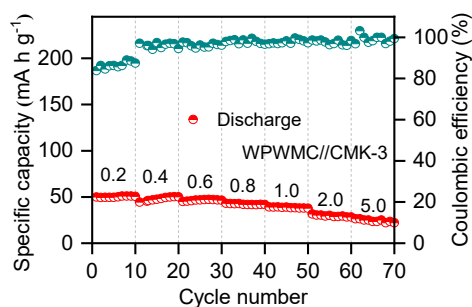


Fig. S27. The rate capabilities at various current rates of the WPWMC//CMK-3 PIHC.

Reference

- 1 A. Sadezky, H. Muckenhuber, H. Grothe, R. Niessner, U. Pöschl, *Carbon*, 2005, **43**, 1731-1742.
- 2 B. Lee, M. Kim, S. Kim, J. Nanda, S. J. Kwon, H. D. Jang, D. Mitlin, S. W. Lee, *Adv. Energy. Mater.*, 2020, **10**, 1903280.
- 3 Y. Qian, Y. Li, Z. Pan, J. Tian, N. Lin, Y. Qian, *Adv. Funct. Mater.*, 2021, **31**, 2103115.
- 4 W. Weppner, R. A. Huggins, *J. Electrochem. Soc.*, 1977, **124**, 1569.
- 5 K. M. Shaju, G. V. S. Rao, B. V. R. Chowdari, *Electrochim. Acta.*, 2003, **48**, 2691-2703.